A Modified BPaL Regimen for Tuberculosis Treatment replaces Linezolid with Inhaled Spectinamides

Malik Zohaib Ali [1,2,6], Taru S. Dutt [1,2], Amy MacNeill [2], Amanda Walz [1,2], Camron Pearce [1,2,6], Ha Lam[1,2], Jamie Philp[1,2], Johnathan Patterson[1,2], Marcela Henao-Tamayo[1,2], Richard E. Lee [3], Jiuyu Liu [3], Gregory T. Robertson [1,2], Anthony J. Hickey [4], Bernd Meibohm [5], Mercedes Gonzalez-Juarrero [1,2]

[1]Mycobacteria Research Laboratories, Colorado State University, 80523, USA

[2] Microbiology, Immunology and Pathology, Colorado State University, 80523, USA

[3] Department of Chemical Biology and Therapeutics, St. Jude Children's Research Hospital, 38105, USA

[4]Technology Advancement and Commercialization, RTI International, 27709, USA

[5] Department of Pharmaceutical Sciences, University of Tennessee Health Science Center, 38163, USA

[6] Program in Cell & Molecular Biology, Colorado State University, 80523, USA

Keywords: mycobacterium tuberculosis, inhalation, spectinamides , BPaL, linezolid, MDR-TB, XDR-TB, therapy, multidrug regimen , C3HeB/FeJ mice , BALB/c mice , 1599

Corresponding Author Information: Mercedes.gonzalez-juarrero@colostate.edu

Abstract

The Nix-TB clinical trial evaluated a new 6-month regimen containing three-oral-drugs; bedaquiline (B), pretomanid (Pa) and linezolid (L) (BPaL regimen) for treatment of tuberculosis (TB). This regimen achieved remarkable results as almost 90% of the multidrug resistant (MDR) or extensively drug resistant (XDR) TB participants were cured but many patients also developed severe adverse events (AEs). The AEs were associated with the long-term administration of the protein synthesis inhibitor linezolid. Spectinamide 1599 is also a protein synthesis inhibitor of *Mycobacterium tuberculosis* with an excellent safety profile but which lacks oral bioavailability. Here, we propose to replace L in the BPaL regimen with spectinamide (S) administered via inhalation and we demonstrate that inhaled spectinamide 1599, combined with BPa —BPaS regimen—has similar efficacy to that of BPaL regimen while simultaneously avoiding the L-associated AEs. The BPaL and BPaS regimens were compared in the BALB/c and C3HeB/FeJ murine chronic TB efficacy models. After 4-weeks of treatment, both regimens promoted equivalent bactericidal effect in both TB murine models. However, treatment with BPaL resulted in significant weight loss and the complete blood count suggested development of anemia. These effects were not similarly observed in mice treated with BPaS. BPaL and BPa, but no the BPaS treatment, also decreased myeloid to erythroid ratio suggesting the S in the BPaS regimen was able to recover this effect. Moreover, the BPaL also increased concentration of proinflammatory cytokines in bone marrow compared to mice receiving BPaS regimen. During therapy both regimens improved the lung lesion burden, reduced neutrophil and cytotoxic T cells counts while increased the number of B and helper and regulatory T cells. These combined data suggest that inhaled spectinamide 1599 combined with BPa is an effective TB regimen that avoids L-associated AEs.

IMPORTANCE Tuberculosis (TB) is an airborne infectious disease that spreads via aerosols containing *Mycobacterium tuberculosis* (Mtb), the causative agent of TB. TB can be cured by administration of 3-4 drugs for 6-9 months but there are limited treatment options for patients infected with multidrug (MDR) and extensively resistant (XDR) strains of Mtb. BPaL is a new all-oral combination of drugs consisting of Bedaquiline (B), Pretomanid (Pa) and Linezolid (L). This regimen was able to cure ~90% of MDR and XDR TB patients in clinical trials but many patients developed severe adverse events (AEs) associated to the long-term administration of linezolid. We evaluated a new regimen in which Linezolid in the BPaL regimen was replaced with inhaled spectinamide 1599. In the current study, we demonstrate that 4-weeks of treatment with inhaled spectinamide 1599 in combination with Bedaquiline and Pretomanid has equivalent efficacy to the BPaL drug combination and avoids the L-associated-AEs.

64 **Introduction**

65 Tuberculosis (TB) remains one of the leading causes of death initiated by an
66 infectious agent. In 2021, the World Health Organization reported 10.6 million new TB
67 cases worldwide and among those, 450,000 cases were also diagnosed as multidrug
68 resistant (MDR) or extensively drug resistant (XDR) TB (1). Treatment of MDR- and XDR-
69 TB patients is lengthy and is often poorly tolerated due to significant associated side
70 effects (2).

71 Recently, a 6-month novel treatment regimen of three-oral-drugs: bedaquiline (B),
72 pretomanid (Pa) and linezolid (L) referred to as the BPaL regimen was approved.
73 Preclinical studies demonstrated the better efficacy of BPaL regimen for drug sensitive
74 TB compared to the standard TB chemotherapy (1,3,4) and thereafter, the BPaL regimen
75 was tested in the Nix-TB clinical trial conducted in South Africa (5). This trial enrolled
76 patients with XDR-TB and treatment-intolerant or non-responsive MDR-TB, including HIV
77 positive patients with a CD4 count of 50 or higher. The results were remarkable as 95 out
78 of 107 patients were cured though many patients had a high rate of treatment-associated
79 adverse events (AEs).

80 The long-term administration of linezolid (an oxazolidinone antibiotic) was likely
81 the causative agent resulting in bone marrow myelosuppression (48%), peripheral
82 neuropathy, optic neuritis (81%) and anemia (37%) in patients treated with the BPaL
83 regimen (5). Subsequently, the ZeNix trial adjusted the BPaL regimen to a linezolid dose
84 of 600mg. This trial also had remarkable results; it cured 84-91% of patients (9 to 26
85 weeks of therapy, respectively) and resulted in fewer AEs than those observed in the Nix-
86 TB trial (6). Apart from AEs, several studies have also raised awareness of high doses of

87 linezolid leading to development of linezolid-resistant *Mycobacterium tuberculosis* (Mtb)
88 (7–9). At present, the TB-drug development field is working to modify the BPaL regimen
89 to maintain or improve its efficacy while diminishing treatment-associated AEs (10).

90 Spectinomycin, an aminocyclitol antibiotic, is a broad spectrum antibiotic used
91 mainly for the treatment of *Neisseria gonorrhoeae* (11). It inhibits bacterial protein
92 synthesis (12) and has an acceptable safety profile with no known ototoxicity and
93 nephrotoxicity (13,14). The activity of spectinomycin against Mtb is very poor but its
94 structural modification led to the development of a new series of semisynthetic analogs
95 called spectinamides (12,15,16). Spectinamides bind selectively with the bacterial 30S
96 ribosomes and importantly, unlike linezolid, they do not bind to the mitochondrial 30S in
97 mammalian cells. The latter represents a great advantage for reduced potential for side
98 effects, such as ototoxicity and myeloid suppression that are commonly associated with
99 other protein synthesis inhibitors such as amikacin and linezolid, respectively (17,18).
100 Spectinamides' potent anti-tubercular activity is attributed to its ability to evade drug efflux
101 by Rv1258c major facilitator superfamily transporter present on the surface of Mtb
102 (19,20). Spectinamides have shown excellent activity against MDR- and XDR-Mtb strains
103 (16,21) h owever, their poor oral availability has limited their usage to injectable forms.

104 One of the lead spectinamides, 1599, has demonstrated promising results *in vitro*
105 and *in vivo* and was shown to lack cross-resistance with existing anti-TB drugs (16,19–
106 23). 1599, delivered subcutaneously, proved an effective partner agent when combined
107 with rifampin and pyrazinamide and also with bedaquiline, pretomanid or moxifloxacin in
108 TB mouse efficacy models of increasing complexity (21).

109 One of the limitations of using 1599 as injectable is a potential risk for poor
110 patient compliance (24) and direct administration of aerosolized antibiotics to the lungs
111 has been studied for decades as an alternative to systemic drug administration via
112 injection. Aerosolized administration of 1599 has been tested in preclinical *in vivo*
113 studies using liquid formulation of the drug. These studies have shown that inhaled
114 1599, used in monotherapy or in combination with pyrazinamide, is efficacious and well
115 tolerated in murine TB efficacy models (25,26). A comparative study assessing
116 biodistribution of the drug in relation to the administration route demonstrated that 1599
117 showed 48 times higher exposure in mouse lungs via inhalation compared to equivalent
118 dosages administered by subcutaneous injection; the latter may explain the increased
119 efficacy of this drug following intrapulmonary aerosol (22,26). Moreover, 1599 was
120 shown to be amenable to dry powder formulation and delivery, suggesting a pathway to
121 a more patient-friendly delivery system (27). Therefore, in this study, we hypothesized
122 that combining BPa with inhaled S will maintain equivalent efficacy to the BPaL regimen
123 while avoiding the accompanying toxicities that occurred with long-term BPaL
124 administration to human MDR/XDR-TB patients. Based on the diversity of outcomes
125 observed during human TB disease (22) and as no single animal model recapitulates
126 the wide spectrum of human TB pathology (28), we chose the BALB/c and C3HeB/FeJ
127 murine TB models. The BALB/c chronic TB model is representative of a long-term Mtb
128 chronic infection that develops homogenous lung granulomatous lesions restraining the
129 bacilli within intracellular compartments (29) of macrophages and foamy macrophages.
130 In contrast, low-dose aerosol Mtb infection of C3HeB/FeJ mice also results in a chronic
131 infection, but their lungs exhibit a heterogenous spectrum of lesions including

132 granulomas similar to those seen in BALB/c chronic TB model in addition to caseous
133 necrotic lesions surrounded by a fibrotic rim (30–32). The caseum of these necrotic
134 granulomas creates a hypoxic environment and contains abundant extracellular bacilli
135 (31–33) in a similar fashion to necrotic granulomas found in some human TB patients. It
136 is believed that the fibrotic, necrotic and hypoxic environment of these granulomas
137 creates barriers to drug penetration, alters bacterial phenotype, and all together
138 challenge therapeutic outcomes (34–37). Therefore, to understand the implications of
139 drug efficacy and drug associated AEs in scenario without (BALB/c) and with
140 (C3HeB/FeJ) necrotic granulomas, both murine TB efficacy models were employed.
141

142 **Results**

143 ***Linezolid and spectinamide 1599 show similar efficacy in monotherapy***

144 To compare the efficacy of L or S in monotherapy, Mtb-infected C3HeB/FeJ (n=7)
145 and BALB/c (n=4-6) mice received L (administered 5/7 days per week orally at 100
146 mg/Kg) or S (administered 3/7 days per week on alternate days via intrapulmonary
147 aerosol delivery at 100 mg/Kg and 50 mg/Kg, respectively) for 4 weeks. At the end of
148 treatment, the animals were sacrificed, and the CFU in lungs and spleen was enumerated
149 (Figure 1A-D). Treatment of C3HeB/FeJ mice with L (7.30 ± 0.45 $\log_{10}$) or S (6.90 ± 0.48
150 $\log_{10}$) for 4 weeks resulted in an average of 0.51 and 0.91 $\log_{10}$ CFU reduction in the
151 lungs respectively, compared to untreated (UnRx) control (7.81 ± 0.36 $\log_{10}$) (Figure 1A).
152 This difference failed to achieve statistical significance owing to the larger standard
153 deviation associated with heterogenous advanced lung pathology observed in this model
154 (26,31,32). In contrast, L (4.49 ± 0.10 $\log_{10}$) treated C3HeB/FeJ mice had significantly

155 lower spleen bacterial burden compared to UnRx (5.43 ± 0.27 log_{10}), with no significant
156 difference between the L and S (4.94 ± 0.11 log_{10}) treatment arm (Figure 1C). In BALB/c
157 mice, L or S treatment was found to promote significant reduction in lung bacterial burden
158 (0.83 and 0.77 log_{10} respectively) compared to UnRx or the vehicle only controls (Figure
159 1B). There was no significant difference in lung bacterial burden after L or S treatment in
160 BALB/c mice and there was no change in spleen bacterial burden compared to UnRx
161 control (Figure 1D).
162
163 ***Combination therapy with BPaL or BPaS have similar efficacy***
164 We further tested and compared the efficacy of L or S when used in combination
165 therapy with BPa. Mtb-infected C3HeB/FeJ mice were treated with either BPaL (B=
166 25mpk; Pa= 100 mg/Kg and L= 100 mg/Kg all administered 5/7 a week via oral gavage)
167 or BPaS (BPa as in BPaL and S= 100 mg/Kg administered 3/7 a week on alternate days
168 via intrapulmonary aerosol delivery) for 4 weeks. The comparative analysis from
169 combined data of three independent studies is shown in Figure 1E&G (data from
170 individual studies are shown in Figures S1-3). Two of three studies contained an extra
171 group of BPa treated mice as a reference control. Compared to UnRx (7.48 ± 0.12 log_{10})
172 control, mice in the BPa (5.49 ± 0.42 log_{10}), BPaL (4.76 ± 0.38 log_{10}) and BPaS (4.98 ±
173 0.35 log_{10}) treatment groups had significantly reduced the lung bacterial burden by 1.99,
174 2.72, and 2.50 log_{10} respectively (Figure 1E). Although a higher CFU reduction was
175 observed in the lungs of C3HeB/FeJ mice treated with BPaL or BPaS, these differences
176 failed to achieve statistical significance compared to BPa backbone regimen. All three
177 regimens proved highly effective at reducing spleen bacterial burden in C3HeB/FeJ mice,

178 with most mice returning no CFU within the limit of detection (LOD) employed herein
179 (Figure 1G).

180 The effect of BPaL and BPaS (S= 50 mg/Kg) combination therapy on the bacterial
181 burden in lungs and spleen of Mtb-infected BALB/c mice was determined at the end of 4-
182 weeks of treatment. Figure 1F&H show the combined lung and spleen CFU data from two
183 independent studies (data for each study is shown in Figures S8-9). The combined result
184 demonstrated that compared to UnRx (5.24 ± 0.17 $\log_{10}$) control, mice in the BPaL (1.29
185 ± 0.13 $\log_{10}$) and BPaS (1.44 ± 0.17 $\log_{10}$) treatment groups returned significantly fewer
186 CFU in the lungs, with most mice returning no CFU within the LOD employed herein
187 (Figure 1F). As in C3HeB/FeJ TB model, no significant difference was observed in the
188 lung CFU of BALB/c mice treated with either the BPaL or BPaS regimen. BPaL and BPaS
189 therapy reduced BALB/c spleen bacterial burden to below the LOD of the assay with no
190 CFU recovered for any treated mice (Figure 1H). In summary, these results support our
191 hypothesis and demonstrate that both BPaL, BPaS (and BPa in the C3HeB/FeJ TB
192 model) multidrug regimens show equivalent bactericidal effects in C3HeB/FeJ and
193 BALB/c chronic TB efficacy models.

194

195 **Monitoring of adverse events**

196 Five approaches were employed to monitor treatment-associated AEs in mice in
197 this study including 1) changes in the body weight of mice; 2) lung histopathology and
198 lesion scoring; 3) evaluation of complete blood count (CBC); 4) clinical pathology to
199 study myelosuppression in bone marrow and 5) changes in content of immune cells in
200 the lungs, spleen, bone marrow and blood.

201 ***BPaL therapy decreases the*** body weight ***of mice***

202 No significant difference in the body weight among the treatment groups in either
203 C3HeB/FeJ or BALB/c mice was observed following 4-weeks of treatment with S or L
204 alone (Figure S4A and S10A respectively). On the other hand, C3HeB/FeJ or BALB/c
205 mice treated with BPa, BPaL or BPaS showed marginal loses of body weight, ranging
206 from 2.37-5.13% and only mice receiving the BPaL regimen, when compared to the UnRx
207 control, reached statistically significant loses in body weight by the end of treatment
208 (Figure S4B and S10B respectively).

209

210 ***BPaL and BPaS therapy result in significant lower lung lesion burden***

211 The lesions in Mtb-infected UnRx C3HeB/FeJ mice (Figure 2A&B) showed a
212 spectrum of diverse granuloma types ranging from aggregations of macrophages and
213 lymphocytes to highly organized granulomas with collagen encapsulation and a region
214 of central caseous necrosis that resembles to those found in some human patients
215 (31,32). By comparison, lung lesions of Mtb-infected UnRx BALB/c mice (Figure 2C&D)
216 consisted of granulomas with a very homogeneous structure (31) formed also by
217 aggregations of macrophages and lymphocytes without a necrotic core. Mice treated for
218 4 weeks with the BPaL or BPaS regimen presented with significant reduction in the
219 number and size of granulomas in both C3HeB/FeJ and BALB/c TB models compared
220 to their respective UnRx control, with no significant difference in lesion burden score
221 between the combination drug treatment groups (Figure 2E&F).

222

223

224 ***Association of L with altered blood profile and mild anemia in mice***

225 The effect of L in the blood profile of humans and mouse has been reported (38–
226 42) but the same has not been reported for S. Therefore, a complete blood count (CBC)
227 profile was performed on Mtb-infected C3HeB/FeJ mice at the end of 4-weeks of
228 treatment to quantify treatment-associated hematological changes. The results obtained
229 from mice treated with L or S alone are summarized in Figure 3A. Of 20-blood parameters
230 evaluated, two blood parameters were affected during treatment. When compared to
231 UnRx control and S treated mice, L treatment significantly increased the red blood cell
232 distribution width standard deviation (RDWs), while both L and S treatment were
233 associated with a significant decrease in the mean corpuscular hemoglobin concentration
234 (MCHC) compared to UnRx control (Figure 3A).

235 The Nix-TB trial associated the long-term administration of L within the BPaL
236 regimen as the causative agent resulting in anemia in patients treated with the BPaL
237 regimen (5). Thus, the effect of combination therapy with the BPaL or BPaS regimen on
238 CBC profile was analyzed at 1-, 2- and 4-weeks of treatment (Figure 3B). None of the 20
239 parameters of CBC changed during the first 2 weeks of treatment. However, out of the
240 20-blood parameters evaluated, a total of four blood parameters were affected at 4-
241 weeks-of treatment. L-containing BPaL regimen was again associated with a significant
242 increase in the RDWs, and lower hemoglobin (HGB) compared to UnRx control after 4
243 weeks. This effect was not observed in mice treated with BPa or BPaS (Figure 3B).
244 However, as in monotherapy, there was a trend towards lower overall MCHC in mice
245 treated with either BPaL or BPaS. The mean platelet volume (MPV) was marginally higher
246 at 4 weeks in mice treated with BPa compared to BPaL or BPaS, albeit not significantly

247 different from UnRx control (Figure 3B). Given that no difference in HGB or RDWs was
248 observed between UnRx control and their comparator BPa and BPaS regimens, we
249 concluded that the significant HGB decrease and RDWs increase (often observed during
250 development of anemia) were associated with inclusion of L in BPaL regimen.
251
252 ***Spectinamide 1599 recovers the altered ratio of myeloid to erythroid cells in bone***
253 ***marrow***
254 To further evaluate if L was associated with myelosuppressive effect, we
255 performed hematopathology analysis on bone marrow from Mtb-infected C3HeB/FeJ and
256 BALB/c mice at the end of treatment. For C3HeB/FeJ mice, the number of myeloid (M)
257 and erythroid (E) precursor cells were calculated from H&E stained sections and their
258 myeloid-to erythroid ratio (M:E) was determined by counting 300 bone marrow cells in 5
259 different regions (Figure 3C). The BPa and BPaL treatment significantly decreased
260 myeloid cells while increasing the proportion of erythroid cells (Figure 3D). Hence, the
261 corresponding ratio in bone marrow of animals treated with BPaL or BPa was lower
262 compared to UnRx control. Importantly, the BPaS treatment did not show any difference
263 in the content of myeloid or erythroid cells when compared to UnRx control suggesting
264 that S in the BPaS was able to recover this effect. In Mtb-infected BALB/c mice, the
265 number of myeloid and other cell types were counted, however, no significant difference
266 was found among the control and treatment groups (data not shown).
267
268

269 ***BPaL therapy increases proinflammatory cytokine response in bone marrow***

270 A comparative analysis for concentration of cytokines and chemokines in the bone
271 marrow, plasma, and lung samples from Mtb-infected C3HeB/FeJ mice treated with BPaL
272 or BPaS regimen was also conducted. The bone marrow samples demonstrated a
273 significant difference between the BPaL and BPaS groups, with appreciably higher level
274 of pro-inflammatory cytokines and chemokines (IL-1β, IL-12p70, IL-23, TNFα, GROα
275 (CXCL1), MP-2α (CXCL2), IP-10 (CXCL10), MP-1α (CCL3), RANTES (CCL5), MCP-3
276 (CCL7) and Eotaxin (CCL11)) in the BPaL- compared to BPaS-treated mice (Figure 4B).
277 The plasma and lung samples, however, had similar cytokine and chemokine contents
278 between the treatment groups except for MCP-3 (CCL7) in plasma which was significantly
279 higher in BPaS compared to BPaL group (Figure S13). We also performed a correlation
280 analysis of bone marrow cytokine and chemokine content with lung CFU obtained from
281 treatment (BPaL or BPaS) and UnRx groups (Figure 4C). The analysis suggested that
282 compared to UnRx control, there was a strong correlation between the profound reduction
283 of lung bacterial burden and profound reduction in bone marrow cytokine and chemokine
284 contents observed in mice from BPaL or BPaS groups. Similar correlations were found
285 between lung CFU and content of cytokines and chemokines in lung (Figure S14) and
286 plasma (Figure S15).

287

288 ***BPaL and BPaS therapies reduce inflammation-associated cells***

289 We further assessed the environment of immune cells using flow cytometry in
290 bone marrow, lungs, and blood from each group of Mtb-infected C3HeB/FeJ mice
291 (Figure 5). The bone marrow (Figure 5A) results revealed that as compared to UnRx

292 control, there was a significant decrease in the percentage of inflammatory myeloid
293 phenotypes (CD45+CD3-CD11b+CD11c-Ly6C+CCR2+, CD45+CD3-CD11b+CD11c-
294 Ly6C+CCR2+MHC-II+ and CD45+CD3-D14+CCR2+) in response to therapy with either
295 BPa, BPaL, or BPaS. In contrast, neutrophils (CD45+CD3-CD11b+CD11c-
296 Ly6C+Ly6G^{high}), precursor T cells (CD45+CD3+) and B cells (CD45+CD3-CD19+B220-)
297 were significantly increased in either BPa, BPaL, or BPaS treatment groups compared
298 to UnRx control in bone marrow. This reduced inflammatory response in treatment
299 groups is also consistent in blood shown by significantly reduced inflammatory myeloid
300 cells (CD45+CD3-CD11b+CD11c-Ly6C+CCR2+) (Figure 5B). Interestingly, the
301 response to therapy in the lungs (Figure 5C) was manifested by a significant increase of
302 CD3+CD4+ T helper cells and B-1 cells (CD3-CD19+) and a reverse trend for
303 CD3+CD8+ and γδ-T cells (CD3+CD8+γδTCR+).
304 Furthermore, we also assessed changes in the distribution of immune cells in the
305 lungs from Mtb-infected C3HeB/FeJ mice in response to therapy using multiplex
306 fluorescent immunohistochemistry (mfIHC). A 7-color composite image for cell markers
307 (B220, CD4, CD8, Foxp3, F4/80 and Ly6G) along with DAPI is shown in Figure 6A,
308 while their single-color staining is shown in Figure 6B. Figure 6A shows a typical
309 necrotic TB granuloma comprised of central necrosis, peripheral rim and lung
310 parenchyma. The analysis of mfIHC images revealed that the BPaL and BPaS
311 treatments significantly and dramatically lowered the number of neutrophils (count
312 based on Ly6G+) compared to UnRx control, however, F4/80+ cells were observed
313 significantly higher in BPaS compared to UnRx control (Figure 6C, S16). Interestingly,
314 the spearman's correlation plot (Figure 6D) shows that a significant decrease in

315 neutrophils was positively correlated with the corresponding increase in most of the
316 other immune cells.
317
318 **Discussion**
319 We used two preclinical chronic TB murine efficacy models (34–36) to investigate
320 BPa, BPaL and BPaS, for efficacy and any associated AEs during the course of 4-
321 weeks of treatment. Overall, our antimicrobial data are in accordance with the
322 granuloma spectrum of both mouse models used where a more robust reduction in lung
323 bacterial burden was observed in the absence (BALB/c) versus the presence
324 (C3HeB/FeJ) of necrotic lesions. Both multidrug regimens as BPaL or BPaS
325 significantly reduced lung bacterial burden by 3.8-4.0 $\log_{10}$ and 2.5-2.7 $\log_{10}$ in BALB/c
326 and C3HeB/FeJ TB models, respectively (Figures 1E-H). We therefore conclude that
327 both regimens promote similar bactericidal effects in murine models lacking, or
328 featuring, advanced pulmonary pathology. Furthermore, the potent antimicrobial effect
329 of the BPaL and BPaS regimens also resulted in improvement of the pathological
330 outcome during chronic infection with Mtb but only the L-containing BPaL regimen, not
331 BPaS, was associated with a significant decrease in the body weight at week 4 in Mtb-
332 infected BALB/c and C3HeB/FeJ mice (Figure S4B and S10B). Future studies will
333 determine if prolonged treatment with BPaL will continue affecting the body weight of
334 the animals. The extent of weight loss is an important preclinical and clinical parameter
335 in TB patients because it determines the severity of disease progression (43), and it is
336 also an indicator of *in vivo* drug efficacy (44). The bactericidal effects of S (as
337 monotherapy) (45) and BPaL (46) in mice observed in these studies is in line with

338 previous reports and similar inverse relationship between body weight and L exposure
339 was recently reported in human patients (47).

340 Among L-associated hematological side effects, the incidence of anemia is
341 reported up to 62.5% in MDR and XDR-TB patients (48–50) and the onset of this effect
342 can occur 2 weeks to 2 months post L administration (38). In TB patients treated with anti-
343 TB drugs (51–53), increased RDWs and lower HGB are associated with anemia and
344 these parameters serve as markers of disease prognosis. Using a CBC profile of 20
345 peripheral blood parameters, our preclinical study failed to detect any difference between
346 L or S 4-weeks monotherapy in terms of total red blood cells, white blood cells, platelets,
347 or hemoglobin (HGB) concentration compared to UnRx control (data not shown).
348 However, L treatment alone increased the RDWs and both L and S decreased the MCHC
349 (Figure 3A). Likewise, none of the 20-blood parameters evaluated showed any change
350 after the first 2 weeks of therapy with BPa, BPaL, or BPaS (Figure 3B). However, by 4
351 weeks, a significant drop in HGB and an increase in the RDWs was apparent for the BPaL
352 group (Figure 3B). This is interpreted to mean that mild hematological effects observed
353 in mice treated for 4 weeks with L or BPaL are dependent on the number of L-doses
354 administered and are thus, time-dependent. Overall, the onset of these hematological
355 effects when testing an L-containing regimen (BPaL) is in agreement with previous
356 studies (38,39) in human patients.

357 The mechanism of L-induced toxicity is attributed to its binding with the host
358 mitochondrial ribosomes leading to mitochondrial toxicities (17). The latter results in
359 activation of Nlrp3 inflammasome (54) and subsequently results in L-mediated bone
360 marrow myelosuppression (55); a phenomenon consistent with the hematologic

361 anomalies seen in patients treated with L for extended time periods. Because
362 spectinamides do not bind to mitochondrial ribosomes there is reduced potential for
363 similar side effects (16,18). To conclusively test this hypothesis, we performed bone
364 marrow histopathology to quantify the myeloid to erythroid ratio (M:E), a parameter that
365 provides information about the relative proportions of myeloid lineage (granulocytes,
366 monocytes, and their precursors) to erythroid lineage (56). The BPa and BPaL regimens
367 altered M:E in the C3HeB/FeJ TB model by suppressing myeloid and inducing erythroid
368 lineages (Figure 3C&D) whereas no such difference was observed in mice treated with
369 BPaS compared to untreated control. L was previously shown to impact M:E ratio,
370 although an opposite trend was observed in those studies, which employed 12-days of
371 L administration and a different strain of otherwise healthy mice (54). Time course
372 studies using a single consistent assay method are needed to resolve this discrepancy.
373 Elevation of interleukin 1β (IL-1β) levels and activation of Nlrp3 inflammasome
374 have been previously linked to myelosuppression (55). A 26-plexed immunoassay on
375 bone marrow samples from Mtb-infected C3HeB/FeJ mice revealed that most of the
376 proinflammatory cytokines and chemokines including IL-1β, IL-12p70 and TNF-α were
377 present at significantly higher concentrations in animals treated with BPaL compared to
378 BPaS (Figure 4A&B). The presence of elevated IL-1β was previously reported during
379 monotherapy with L (54,57). Studies from UnRx Mtb-infected C3HeB/FeJ mice also
380 revealed highly elevated levels of cytokines and chemokines (Figure 4C). As expected,
381 the positive therapeutic effect of BPaL and BPaS (as seen by reduction in bacterial and
382 lesion burden of lungs) also correlated with decreased level of proinflammatory
383 cytokines in bone marrow, lung, and plasma (Figures 4C, S14 and S15 respectively).

384 Similar to changes observed for cytokine profile, the flow cytometry data of bone
385 marrow, blood, and lungs along with quantification of mfIHC lung image analysis
386 revealed a significant change in the percentage of myeloid and lymphoid phenotypes
387 during treatment compared to UnRx control (Figures 5 and 6). Most notably, the
388 therapeutic effect of the BPa, BPaL and BPaS treatments reduced inflammatory
389 myeloid cells expressing CCR2 in blood and bone marrow and reduction in cytotoxic T
390 cells (CD3+CD8+) and γδT cells (CD3+CD8+γδTCR+) in lungs. In addition, BPa, BPaL
391 and BPaS therapy significantly increased the influx of helper T cells (CD3+CD4+),
392 regulatory T cells (Foxp3+) and B cells (CD3-CD19+) in lungs. These results suggest
393 that the combination therapy promotes the immune system's equilibrium by reducing
394 inflammation and enhancing adaptive immune responses.
395 An additional striking finding from this study was a strong concordance between
396 the decrease in lung and spleen bacterial burden and a corresponding decrease in the
397 number of cells expressing the neutrophil associated marker (Ly6G) (Figure 6C&D). An
398 implication of this finding is that the favorable treatment outcomes may promote a
399 corresponding decline in Ly6G neutrophil population as suggested before (58). Among
400 all immune cell phenotypes studied, no differences were found between BPaL and
401 BPaS treated animals and only the F4/80+ cells in the BPaS (but not in the BPaL)
402 treated animals showed significant increase when compared to the UnRx control.
403

404 To conclude, the TB drug development field is working towards developing shorter and safer
405 therapies with a common goal of developing new multidrug regimens of low pill burden that are
406 accessible to patients, of short duration (ideally 2-3 months) and consist of 3-4 drugs of novel

407 mode-of-action with proven efficacy, safety, and limited toxicity. Here we present initial results for
408 new multidrug regimens containing inhaled spectinamide 1599 that are in line with these goals. It
409 is proposed that human use of spectinamides 1599 will be administered using a dry powder
410 formulation delivered by the RS01 Plastiape dry powder inhaler. We already reported on the
411 aerodynamic properties of dry powder spectinamide 1599 within #3 HPMC capsules and
412 delivered from a RS01 Plastiape inhaler device (59). Future studies are already under
413 consideration for funding by NIH-NIAID to understand the pharmacokinetics of mono, binary and
414 ternary combinations of BPaS. These studies also aim to identify the optimal dose level and
415 dosing frequency of each regimen along with their efficacy and relapse free-sterilization potential.
416 Studies are also planned using a model-based pharmacokinetic-pharmacodynamic (PKPD)
417 framework, guided by an existing human BPa PKPD model (61) to find allometric human dose
418 levels, dosing frequencies and treatment durations that will inform the experimental design of
419 future clinical studies.

420 **Materials and Methods**

421 Female C3HeB/FeJ and BALB/c mice at 6-8 weeks of age were purchased from
422 the Jackson Laboratories. All protocols and use of these animals were approved by the
423 Institutional Animal Care and Use Committee (IACUC) at CSU. Animals were infected
424 with a low dose aerosol infection of Mtb (Erdman strain; ATCC 35801) using an
425 inhalation exposure system (Glas-Col, Terre Haute, IN) calibrated to deliver ~50-100
426 colony forming units (CFU) to the lungs (22). Clinical observations (e.g., inactivity, rough
427 fur, hunched posture, increased respiratory rate or effort) were monitored daily and their
428 body weights were taken weekly.

429

430 **Drug preparation and treatment**

431 Bedaquiline fumarate (B) and linezolid (L) were obtained from LKT laboratories,
432 pretomanid (Pa) from ChemShuttle and 1599 (S: dihydrochloride) was provided by Dr.
433 Lee at St. Jude Children's Research Hospital. B was administered at 25 mg/kg. Pa and
434 L were administered at 100 mg/kg each and S was delivered by inhalation in liquid form
435 at 50 and 100 mg/kg to BALB/c and C3HeB/FeJ mice, respectively. The drugs were
436 formulated in weekly batches according to the body weight of the animals, aliquoted for
437 single daily dosing, and stored at 4 °C in the dark.
438 The drugs were prepared and administered as reported previously (21,22). Drug
439 treatment was started 4 weeks post-aerosol infection for BALB/c and at 8-9 weeks post-
440 aerosol infection for C3HeB/FeJ mice to allow time for lung pathology to fully develop.
441 All drugs were administered once daily for 5 days/week for 4 weeks by oral (gavage)
442 administration except S which was administered 3 days/week by intrapulmonary aerosol
443 delivery using the Penn Century microsprayer as reported previously (22). B was
444 administered in the morning, Pa one hour after B and, L and S at least 4 hours after Pa.

445 **Necropsy**

446 After 4-weeks of treatment, C3HeB/FeJ and BALB/c mice were humanely
447 euthanized by CO_2 narcosis. Blood, lungs, spleen, femur and tibia bones were collected
448 from each mouse for further processing and analysis.

449 **Assessment of Efficacy**

450 The efficacy of the treatment was assessed by determining changes in bacterial
451 burden [measured as colony forming units (CFU)] in the lungs and spleen of animals at
452 necropsy. The lungs and spleen were homogenized and prepared as reported
453 previously (22). The lung homogenates were plated onto 7H11 agar plates

454 supplemented with 0.4% activated charcoal to reduce the carryover effect of drugs and
455 incubated at 37 ^{o}C for 6-8 weeks before the final CFU count. The remaining lung
456 homogenate was centrifuged, and the supernatant was collected and stored at -80 °C
457 for evaluation of cytokines and chemokines.

458 **Histopathology and lesion scoring**

459 The lungs were fixed in 4% paraformaldehyde (PFA) for 48 hours then embedded
460 in paraffin for histopathology. Sections from formalin fixed and paraffin embedded (FFPE)
461 tissues were cut at 5 µm, stained with hematoxylin and eosin (H&E) and scanned at 40X
462 magnification using multispectral automated PhenoImager (Akoya Biosciences) for
463 histopathological evaluation. The extent of lung lesion burden was quantified in blinded
464 digital images using an open-source QuPath software for image analysis as described
465 previously (62). For each tissue section, a region of interest (ROI) was generated at low
466 magnification with a custom tissue detecting algorithm using decision forest training and
467 classification to differentiate tissue versus background based on color and area. Lesions
468 were identified within tissue ROIs at high magnification with an additional custom-made
469 algorithm using decision forest training and classification based on staining intensity, color
470 normalization and deconvolution, area, and morphological features. Percent lesion
471 calculations were integrated into the same algorithm and calculated from tissue area and
472 lesion area as designated by the ROI and lesions detected.

473

474 The sternum and one femur were fixed in 4% PFA and processed for histology.
475 To evaluate the myelosuppressive effect of the drugs, bone sections were cut at 5 µm

476 and stained with H&E. The number of myeloid and erythroid cells from 5 different
477 regions of the bone were blinded and then counted by a veterinary clinical pathologist.
478

479 **Bone marrow collection**

480 Briefly, a 0.6 mL sterile Eppendorf tube punctured at the bottom with the help of a
481 26-gauge needle was inserted into a 1.5 mL sterile Eppendorf tube. One end of the
482 epiphysis of the long bones was cut open to expose the bone marrow and placed down
483 into the small Eppendorf tube-system. The tubes were centrifuged at 10,000 x g for 15
484 seconds and the marrow was collected from the base of the large Eppendorf tube. The
485 bone marrow was resuspended in PBS and centrifuged again. Thereafter, the
486 supernatant was collected and stored at -80 °C for evaluation of cytokines and
487 chemokines while the bone marrow cells were saved in 4% PFA and freezing media for
488 further use in clinical pathology analysis and flow cytometry, respectively.

489 **Processing of blood**

490 For complete blood count (CBC) analysis of C3HeB/FeJ animals during the
491 treatment, blood was collected in K2-EDTA tubes via submandibular vein puncture as
492 described previously (63). The blood was immediately analyzed in VETSCAN® HM5
493 hematology analyzer (Zoetis).

494 At the time of necropsy, whole blood was collected via cardiac puncture in K2-
495 EDTA containing tubes. After adding an equal volume of PBS, the samples were
496 centrifuged at 800 × g for 10 min at 25 °C with the brake off (deceleration = 0). The top
497 plasma layer was collected and stored at -80 °C for evaluation of their cytokine's
498 content. The buffy coat was collected, washed and the erythrocytes were lysed using

499 Miltenyi RBC lysis buffer (Miltenyi, CA). The cells were washed and resuspended in 500
500 µL of complete DMEM media and prepared for flow cytometry analysis.

501 **Cytokine quantification**

502 Multiplex immunoassay was performed using a Luminex bead-based multiplex
503 ELISA kit (ProcartaPlex Mouse Cytokine & Chemokine Panel 1 26plex, reference #
504 EPXR260-26088-901, Invitrogen). Each sample was normalized to the total protein
505 concentration determined by Bicinchoninic acid (BCA) assay (Thermo Fisher). The BCA
506 and Luminex assay were performed according to the manufacturer's instructions and
507 the final stained samples were fixed with 4% PFA prior to acquisition. Sample data were
508 acquired on a MAGPIX instrument running xPONENT 4.3 software (Luminex Corp.).
509 Heatmaps were generated using R pheatmap package. Correlation analysis of cytokine
510 contents in bone marrow, plasma and lungs with the lung bacterial burden was
511 performed using the corrplot package in R.

512

513 **Immune cell populations analysis**

514 Single cell suspension of bone marrow, blood, and lungs from C3HeB/FeJ mice
515 was prepared as described previously (62). Cells counting, viability staining and cell
516 staining (Table S1) was performed accordingly (62). Samples were acquired using
517 Cytek Aurora^{TM} 4-Laser spectral flow cytometer where 100,000 events were recorded.
518 Data were analyzed in FlowJo software (BD Biosciences) using manual gating (64).

519

520 **Multiplex fluorescent immunohistochemistry**

521 Five µm sections of FFPE lung tissues were stained for multiplex fluorescent
522 immunohistochemistry (mfIHC) by the Imaging Core at the University of Colorado,
523 Anschutz Medical Campus, Denver. The mfIHC was performed for a panel of 6-color
524 antibodies + DAPI using Opal-plex Tyramide Signal Amplification (TSA) technique using
525 a Leica Bond III autostainer. The details of antibodies and Opal fluorophores used are
526 given in Table S2. Each antibody was optimized using Opal 3-Plex Anti-Rb Detection Kit
527 (Akoya Biosciences Inc. cat# NEL830001KT) and stained with automated LabSat™
528 Research (Lunaphore Technologies SA, Epredia). Slides were scanned using
529 multispectral automated PhenoImager™ (Akoya Biosciences) and analyzed for several
530 immune cell populations using the inForm® tissue Finder (Version 2.4.8) and
531 Phenochart™ (Version 1.0.12) software (Akoya Biosciences).
532
533 **Statistical analysis.** Bacterial burden data were expressed as CFU which were Log_{10}-
534 transformed and analyzed using GraphPad Prism version 9.5.1 (GraphPad software, La
535 Jolla, CA). The statistical analysis was performed using a Tukey's multiple comparison
536 test as part of either one-way or two-way ANOVA and mixed-model effect where
537 necessary. The correlation analysis was performed using the spearman's correlation
538 test. Flow cytometry and mfIHC data were graphed in R studio and statistical evaluation
539 was performed using stats package in R.

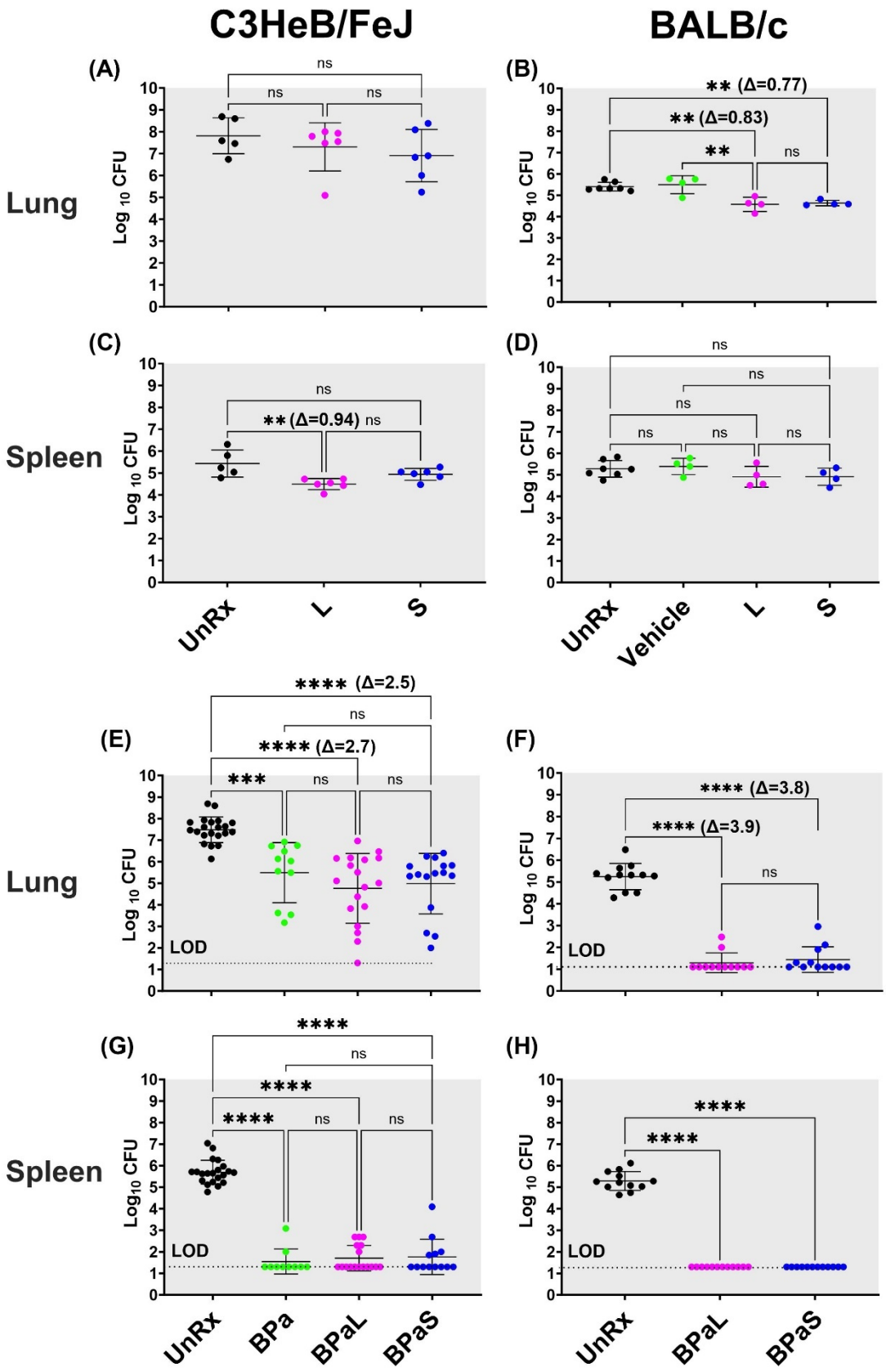
C3HeB/FeJ
BALB/c
(A)
(B)
(C)
(D)
(E)
(F)
(G)
(H)
Lung
Spleen
Lung
Spleen
Log 10 CFU
Log10 CFU
ns
** (Δ=0.77)
** (Δ=0.83)
**
** (Δ=0.94)
**** (Δ=2.5)
**** (Δ=2.7)
***
**** (Δ=3.8)
**** (Δ=3.9)
****
LOD
UnRx
L
S
Vehicle
BPa
BPaL
BPaS

540

541 **Figure 1. Bactericidal effect of BPaL and BPaS in TB mouse models after 4-weeks**
542 **of treatment**

543 BALB/c and C3HeB/FeJ female mice were chronically infected with a low dose aerosol
544 infection of Mtb Erdman strain to deliver ~75 and ~100 bacilli respectively. Post-infection,
545 BALB/c and C3HeB/FeJ mice were rested for 4 and 8-9 weeks respectively until they
546 were randomly assigned to the study groups. The mice were treated with monotherapy
547 of linezolid or spectinamide 1599 or combination therapy of BPaL, BPa or BPaS for 4
548 weeks. Bedaquiline (B), pretomanid (Pa) and linezolid (L) were administered at 25, 100
549 and 100 mg/kg respectively by oral gavage for 5/7 a week while spectinamide 1599 at 50
550 and 100 mg/kg in BALB/c and C3HeB/FeJ TB models respectively for 3/7 a week on the
551 alternate days via intrapulmonary aerosol delivery. On the third day of the last treatment,
552 the mice were euthanized, and their lungs and spleen were collected. The organs were
553 homogenized, serially diluted and plated on 7H11 agar with 4% charcoal (to avoid drug
554 carry-over effect) to determine bacterial burden in the form of colony forming units (CFU)
555 in each sample. CFU were enumerated after 4-6 weeks of incubation at 37 °C and
556 expressed as log_{10}.C3HeB/FeJ and BALB/c TB models showing efficacy of monotherapy
557 (A-D) and combination therapy (E-H). The C3HeB/FeJ graphs (E&G) represent the
558 pooled data from three independent studies (n=3-8 each, Figures S1-3) and two of the
559 three studies contained BPa as a reference control. The BALB/c graphs (F&H) represent
560 the pooled data from two independent studies (n=5 each, Figures S8-9).
561 Statistical significance was calculated using one-way ANOVA with Tukey's multiple
562 comparison test, $p < 0.05$ was considered significant and ** = $p<0.001$, *** = $p<0.0001$,

563 **** = P<0.0001. UnRx = untreated, L = linezolid, S = spectinamide 1599, LOD: limit of

564 detection.

565

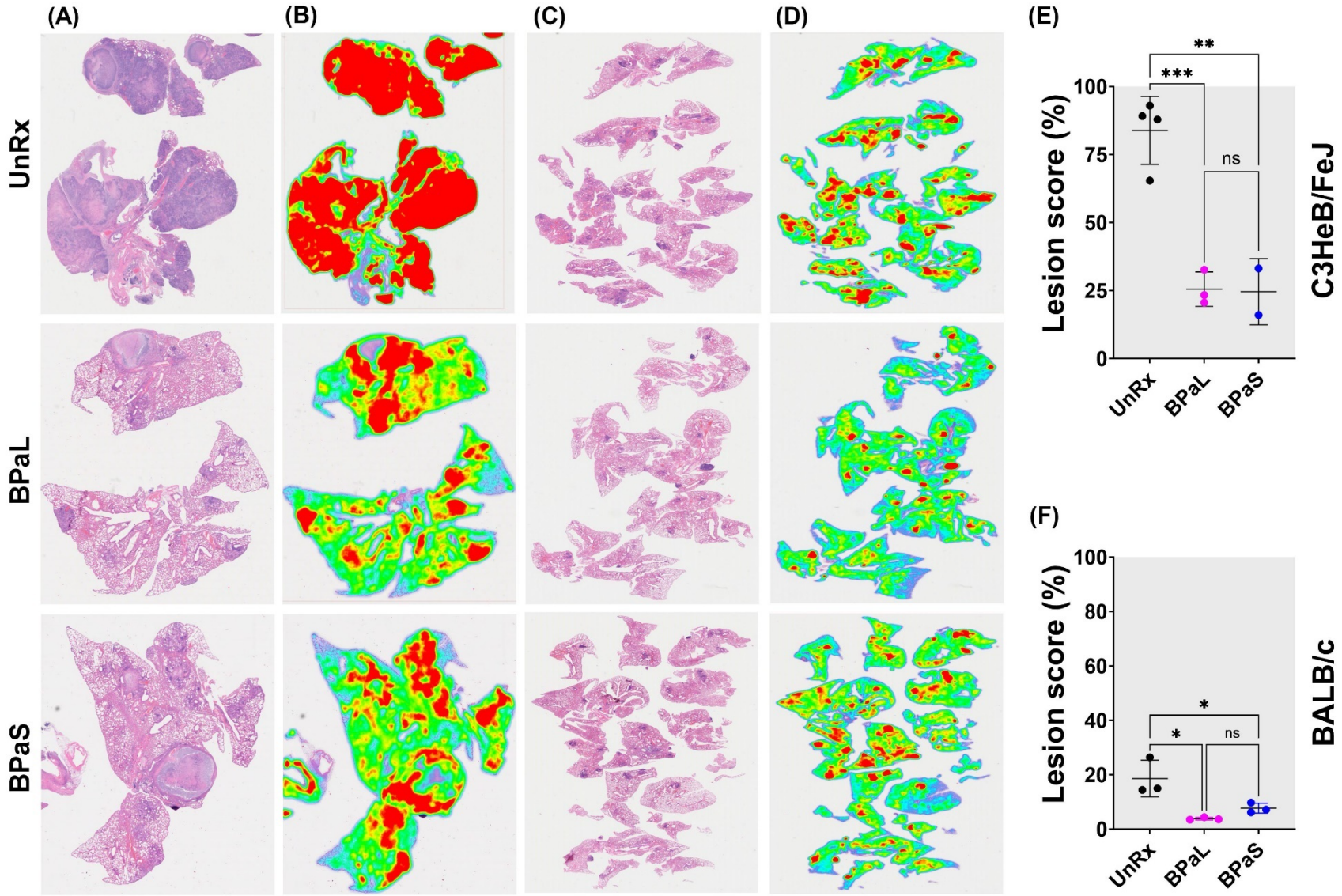
(A)
(B)
(C)
(D)
(E)
(F)
UnRx
BPaL
BPaS
Lesion score (%)
100
75
50
25
0
**
***
ns
UnRx
BPaL
BPaS
C3HeB/FeJ
Lesion score (%)
100
80
60
40
20
0
*
*
ns
UnRx
BPaL
BPaS
BALB/c

566

567 **Figure 2. Effect of therapy on lung histopathology of TB mouse models after 4-**
568 **weeks of treatment.** At the end of therapy, the mice were euthanized, and their lungs
569 were collected and processed for histopathology and lesion scoring. FFPE sections
570 were cut at 5 μm, stained with hematoxylin and eosin (H&E) and imaged at 40x (A:
571 C3HeB/FeJ, C: BALB/c)). Lesion maps (B: C3HeB/FeJ, D: BALB/c) show the infected
572 areas in red color while green color represents the uninvolved parenchymal tissue.
573 Lesion scores (E: C3HeB/FeJ, F: BALB/c) were calculated as the proportion of infected
574 area over the total lung area per animal. Statistical significance was calculated using
575 one-way ANOVA with Tukey's multiple comparison test, and $p < 0.05$ was considered
576 significant and ** = $p<0.001$, *** $P<0.0001$. UnRx = untreated

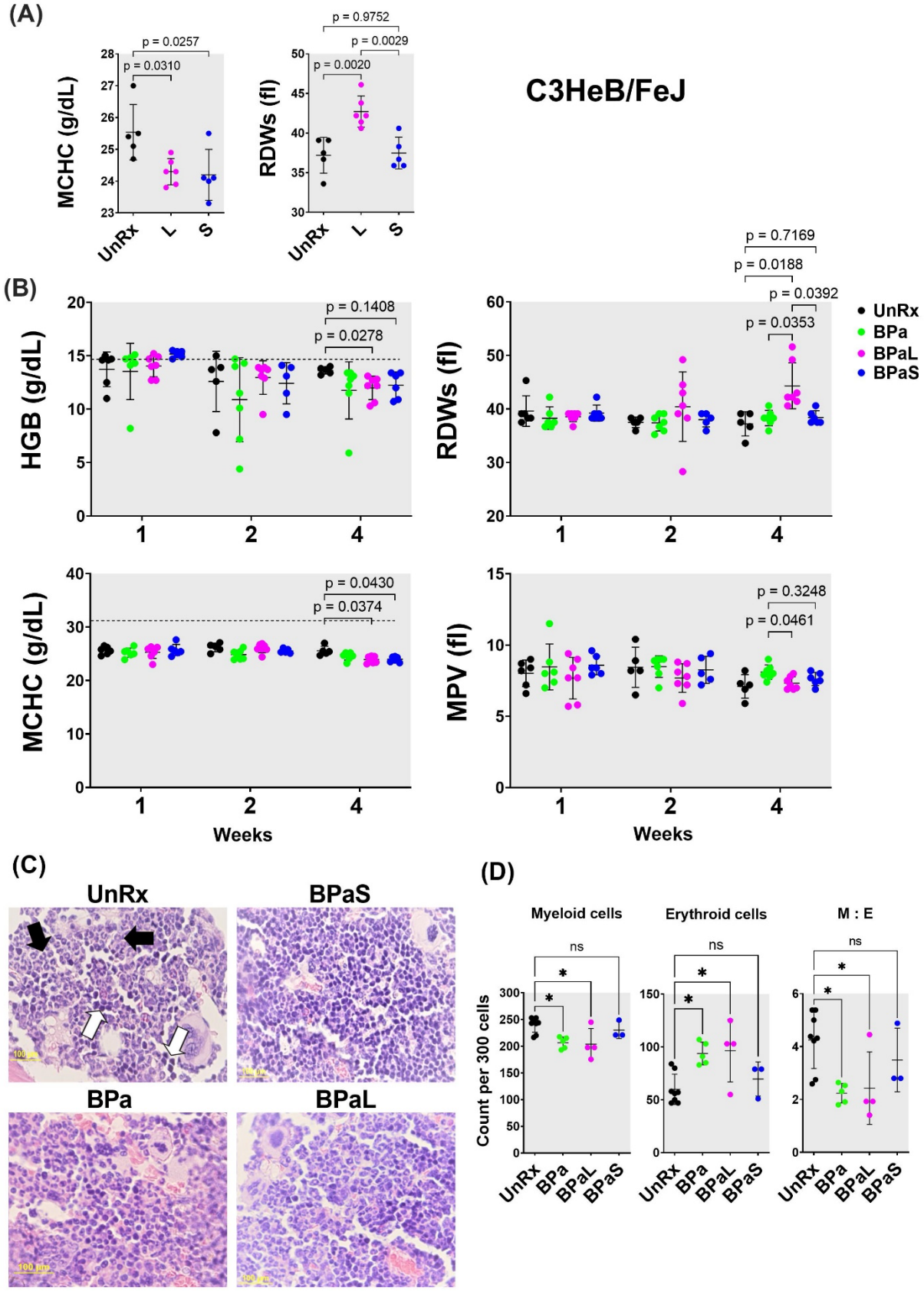
(A)
C3HeB/FeJ
MCHC (g/dL)
p = 0.0257
p = 0.0310
UnRx
L
S
RDWs (fl)
p = 0.9752
p = 0.0029
p = 0.0020
(B)
HGB (g/dL)
p = 0.1408
p = 0.0278
RDWs (fl)
p = 0.7169
p = 0.0188
p = 0.0392
p = 0.0353
UnRx
BPa
BPaL
BPaS
MCHC (g/dL)
p = 0.0430
p = 0.0374
MPV (fl)
p = 0.3248
p = 0.0461
Weeks
(C)
UnRx
BPaS
BPa
BPaL
(D)
Myeloid cells
Erythroid cells
M : E
ns
Count per 300 cells

577

578 **Figure 3. Complete blood count profiling and bone marrow histopathology of Mtb**
579 **infected C3HeB/FeJ TB model during 4-weeks of therapy**
580
581 "During therapy of mice in Figure 1, the blood was collected at 1-, 2- and 4-weeks of
582 treatment. The complete blood count was collected in VETSCAN® HM5 hematology
583 analyzer (Zoetis)". (A) monotherapy, (B) multidrug therapy. The MCHC (mean
584 corpuscular hemoglobin concentration) and RDWs (red blood cell distribution width-
585 standard deviation) along with the HGB (hemoglobin concentration) and MPV (mean
586 platelet volume) are shown. A horizontal dotted line indicates the lower end of the
587 reference interval for C3HeB/FeJ mice.
588
589 The sternum, femur and tibias bones from each mouse were collected, fixed in 4% PFA,
590 and processed for histology (C&D). Sections were cut at 5 μm, stained with hematoxylin
591 and eosin (H&E) and imaged at 40x. (C) Representative photos of bone marrow sections
592 showing myeloid (black arrows) and erythroid (white arrows) cells in bone marrow of
593 untreated (UnRx) and treatment (BPa, BPaS and BPaS) groups. (D) The number of
594 myeloid (M) and erythroid (E) among a total of 300 cells in 5 different regions were
595 counted for each group and M:E was calculated. Statistical significance was calculated
596 using one-way ANOVA with Tukey's test for multiple comparisons. $p < 0.05$ was
597 considered significant and ** = $p<0.001$, *** = $P<0.0001$.

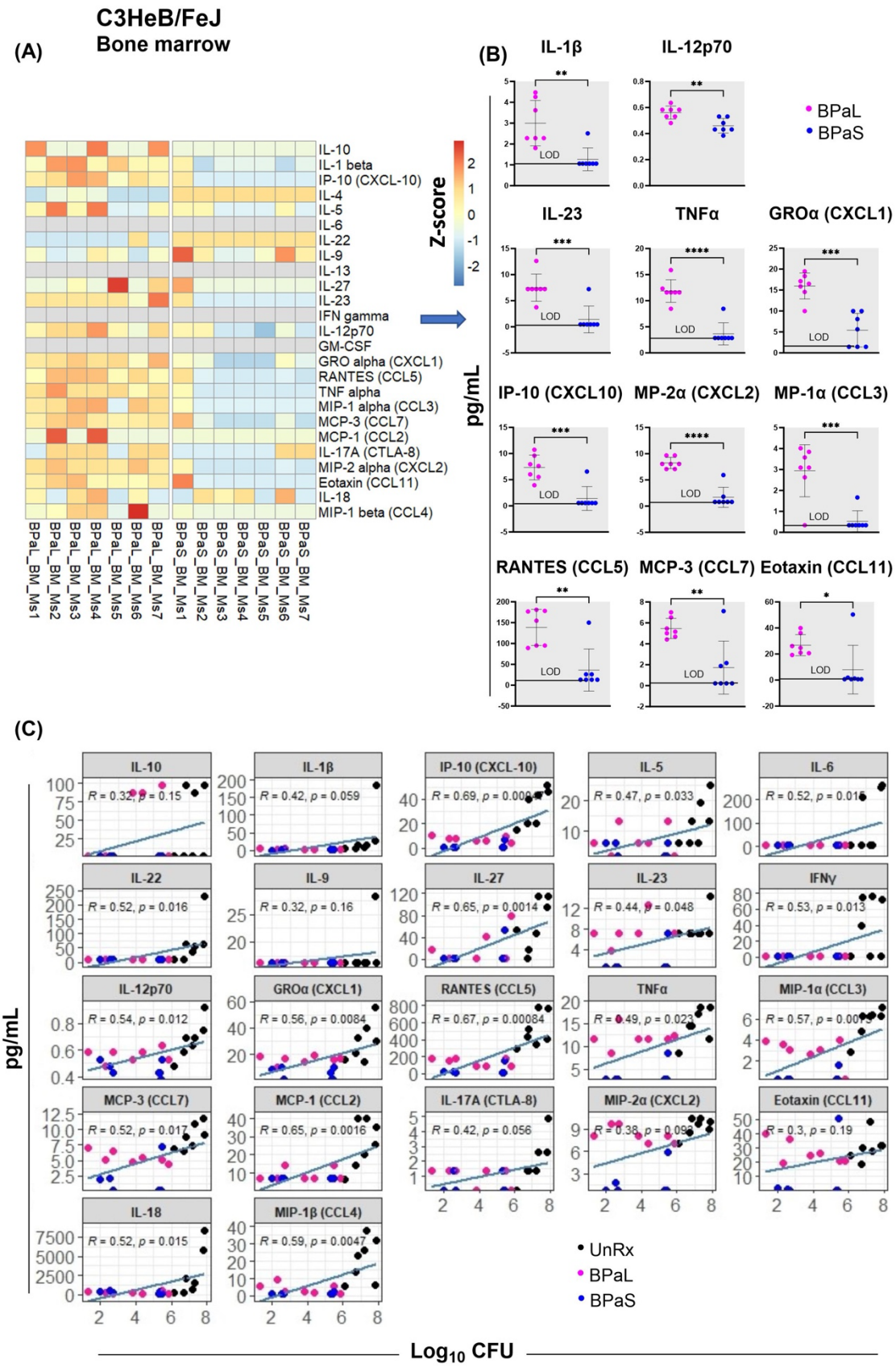
C3HeB/FeJ
Bone marrow
(A)
(B)
(C)
Z-score
IL-10
IL-1 beta
IP-10 (CXCL-10)
IL-4
IL-5
IL-6
IL-22
IL-9
IL-13
IL-27
IL-23
IFN gamma
IL-12p70
GM-CSF
GRO alpha (CXCL1)
RANTES (CCL5)
TNF alpha
MIP-1 alpha (CCL3)
MCP-3 (CCL7)
MCP-1 (CCL2)
IL-17A (CTLA-8)
MIP-2 alpha (CXCL2)
Eotaxin (CCL11)
IL-18
MIP-1 beta (CCL4)
BPaL_BM_Ms1
BPaL_BM_Ms2
BPaL_BM_Ms3
BPaL_BM_Ms4
BPaL_BM_Ms5
BPaL_BM_Ms6
BPaL_BM_Ms7
BPaS_BM_Ms1
BPaS_BM_Ms2
BPaS_BM_Ms3
BPaS_BM_Ms4
BPaS_BM_Ms5
BPaS_BM_Ms6
BPaS_BM_Ms7
BPaL
BPaS
pg/mL
LOD
IL-1β
IL-12p70
IL-23
TNFα
GROα (CXCL1)
IP-10 (CXCL10)
MP-2α (CXCL2)
MP-1α (CCL3)
RANTES (CCL5)
MCP-3 (CCL7)
Eotaxin (CCL11)
IL-10
IL-1β
IP-10 (CXCL-10)
IL-5
IL-6
IL-22
IL-9
IL-27
IL-23
IFNγ
IL-12p70
GROα (CXCL1)
RANTES (CCL5)
TNFα
MIP-1α (CCL3)
MCP-3 (CCL7)
MCP-1 (CCL2)
IL-17A (CTLA-8)
MIP-2α (CXCL2)
Eotaxin (CCL11)
IL-18
MIP-1β (CCL4)
UnRx
BPaL
BPaS
Log10 CFU

598

599 **Figure 4. Bone marrow cytokine and chemokine profiling in Mtb infected**

600 **C3HeB/FeJ TB model after 4-weeks of treatment**

601 Femur bones from selected studies in mice in Figure 1 were collected to harvest the bone
602 marrow. The bone marrow was resuspended in PBS, centrifuged and the supernatant
603 was collected for the evaluation of cytokine's content. BPaL and BPaS therapy showed
604 profile of 26 cytokines and chemokines in bone marrow and the data were converted to
605 Z score and represented as a heatmap (A) and graphically (B). (C) Spearman's
606 correlation analysis of bone marrow cytokines and chemokines (Y axis: pg/ml) with the
607 lung bacterial burden (X axis; log_{10}CFU). Statistical significance was calculated using the
608 t test. $p < 0.05$ was considered significant and ** = $p<0.001$*** = $p<0.0001$, **** =
609 $P<0.00001$.

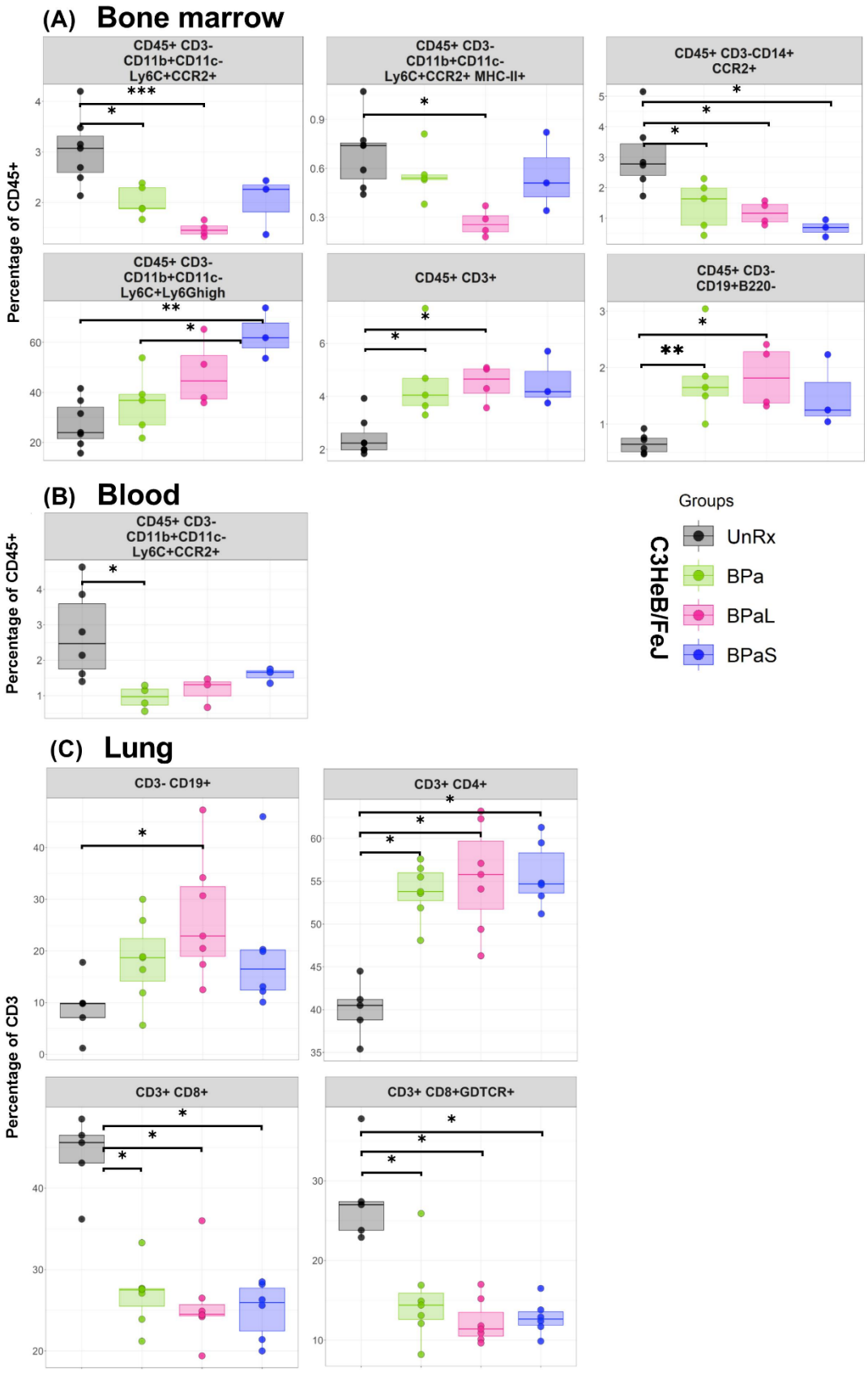
(A) Bone marrow
CD45+ CD3- CD11b+CD11c- Ly6C+CCR2+
CD45+ CD3- CD11b+CD11c- Ly6C+CCR2+ MHC-II+
CD45+ CD3-CD14+ CCR2+
CD45+ CD3- CD11b+CD11c- Ly6C+Ly6Ghigh
CD45+ CD3+
CD45+ CD3- CD19+B220-
Percentage of CD45+
(B) Blood
CD45+ CD3- CD11b+CD11c- Ly6C+CCR2+
Percentage of CD45+
Groups
UnRx
BPa
BPaL
BPaS
C3HeB/FeJ
(C) Lung
CD3- CD19+
CD3+ CD4+
CD3+ CD8+
CD3+ CD8+GDTCR+
Percentage of CD3

638 **Figure 5. Immune cell populations in the bone marrow, lung and blood of**
639 **C3HeB/FeJ TB model after 4-weeks of treatment**

640 The bone marrow, lung and blood from selected studies from Figure 1 were evaluated by
641 flow cytometry. The samples were processed for a panel of 17-color antibodies and the
642 data were analyzed by FlowJo software using manual gating strategy. The myeloid and
643 lymphoid phenotypes present in the untreated (UnRx) and treatment (BPa, BPaL or
644 BPaS) groups are shown. Statistical significance was calculated using one-way ANOVA
645 with Tukey's test for multiple comparisons. $p < 0.05$ was considered significant and ** =
646 $p<0.001$*** = $p<0.0001$, **** = $P<0.00001$.

647

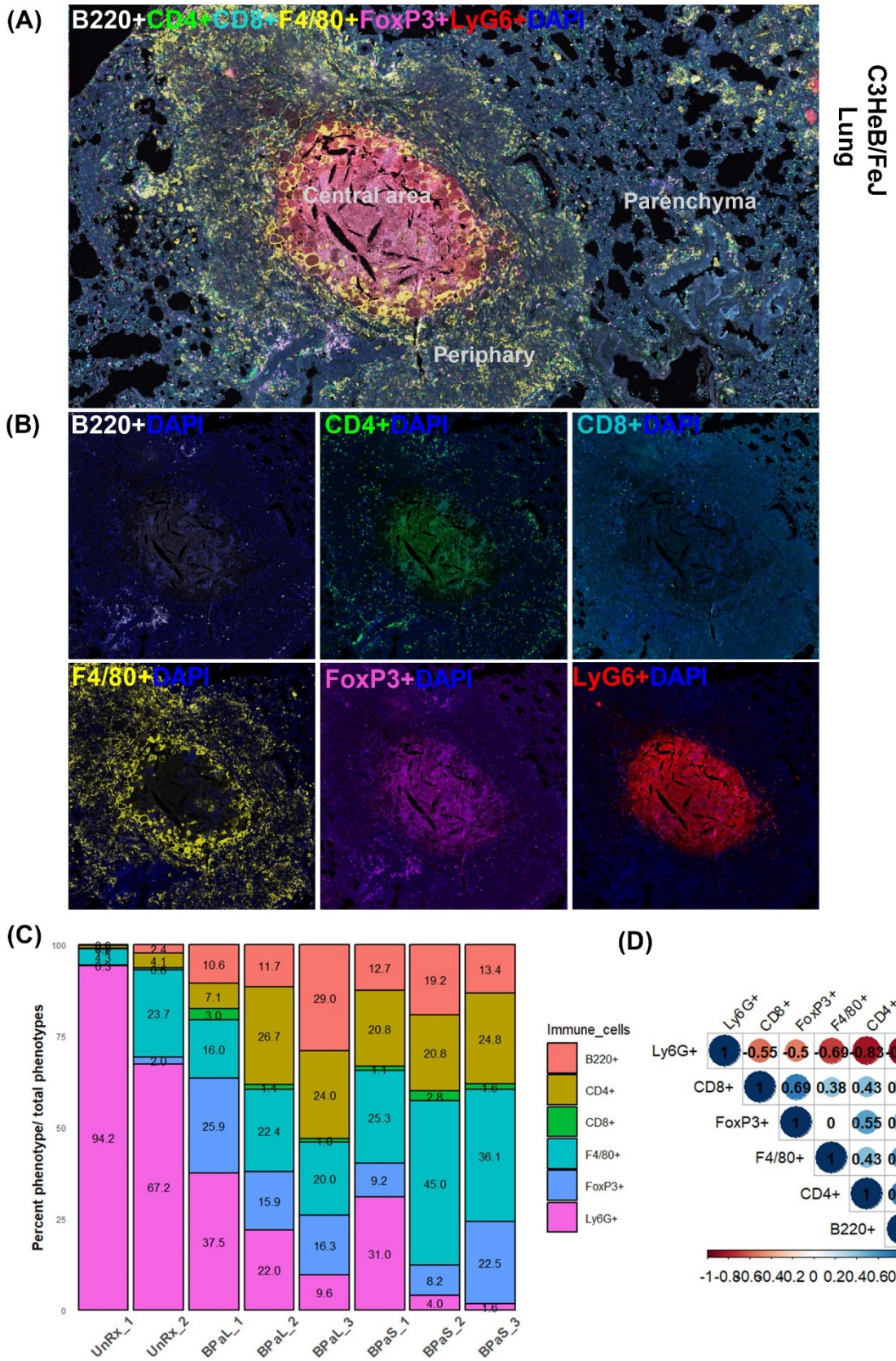
(A)
B220+CD4+CD8+F4/80+FoxP3+LyG6+DAPI
Central area
Parenchyma
Periphary
C3HeB/FeJ
Lung
(B)
B220+DAPI
CD4+DAPI
CD8+DAPI
F4/80+DAPI
FoxP3+DAPI
LyG6+DAPI
(C)
Percent phenotype/ total phenotypes
UnRx_1
UnRx_2
BPaL_1
BPaL_2
BPaL_3
BPaS_1
BPaS_2
BPaS_3
Immune_cells
B220+
CD4+
CD8+
F4/80+
FoxP3+
Ly6G+
(D)
Ly6G+
CD8+
FoxP3+
F4/80+
CD4+
B220+
-1 -0.8 -0.6 -0.4 -0.2 0 0.2 0.4 0.6 0.8 1

648

649 **Figure 6. Immune cell populations in the lungs of Mtb infected C3HeB/FeJ TB**
650 **model after 4-weeks of treatment**
651
652 Selected mice from those shown in Figure 1 were processed for multiplex fluorescence
653 immunohistochemistry (mfIHC). The mfIHC was performed for a panel of 6-color
654 antibodies + DAPI using Opal-plex Tyramide Signal Amplification (TSA). Slides were
655 scanned using multispectral automated PhenoImager™ (Akoya Biosciences) and
656 analyzed for different immune cell populations using the inForm® tissue Finder and
657 Phenochart software (Akoya Biosciences). (A) The lung mfIHC full composite image
658 displays B220, CD4, CD8, F4/80, FoxP3 and Ly6G markers along with DAPI staining for
659 nuclei in the TB granuloma. The central and peripheral regions of a TB granuloma and
660 the parenchyma of lung are also shown. (B) Single color composite image of individual
661 markers with DAPI showing distribution of each immune cell population in the TB
662 granuloma. (C) Cell populations (%) of several immune cells per total number of
663 phenotypes calculated in untreated (UnRx: n = 2 mice) and treatment (BPaL and BPaS:
664 n = 3 mice each) groups based on a panel of 6-color antibodies + DAPI. (D) Spearman's
665 correlation matrix for several immune cell populations (B220, CD4, CD8, F4/80, FoxP3,
666 Ly6G) showing all relationships. A coefficient with a value of either +1 (blue), 0 (white), or
667 -1 (red) indicates a perfect association, no association, and a perfect negative association
668 of ranks, respectively. Numbers indicate the correlation coefficient.

Acknowledgments: This research was supported by the National Institute of Allergy and Infectious Diseases and the Office of the Director of the National Institutes of Health (grants R01AI120670, R01AI090810 and 1S10OD030263 respectively). Dr. Malik Zohaib Ali was a Fulbright Foreign Student Program grantee from Pakistan. Dr. Charles Daley from the Division of Mycobacterial and Respiratory Infections, National Jewish Health, Denver, Colorado 80206, USA advised on current TB drug treatments. The content is solely the responsibility of the authors and does not necessarily represent the official views of the National Institutes of Health. We acknowledge the staff of the Laboratory Animal Resources at Colorado State University for providing animal care.

678 **References**

679 1. Campbell JR, Nsengiyumva P, Chiang LY, Jamieson F, Khadawardi H, Mah HKH,
680 et al. Costs of Tuberculosis at 3 Treatment Centers, Canada, 2010–2016. Emerg
681 Infect Dis. 2022;28(9):1814–23.

682 2. Zhang MW, Zhou L, Zhang Y, Chen B, Peng Y, Wang F, et al. Treatment
683 outcomes of patients with multidrug and extensively drug-resistant tuberculosis in
684 Zhejiang, China. Eur J Med Res. 2021;26(1):1–10.

685 3. Williams K, Minkowski A, Amoabeng O, Peloquin CA, Taylor D, Andries K, et al.
686 Sterilizing activities of novel combinations lacking first- and second-line drugs in a
687 murine model of tuberculosis. Antimicrob Agents Chemother. 2012;56(6):3114–
688 20.

689 4. Tasneen R, Betoudji F, Tyagi S, Li SY, Williams K, Converse PJ, et al.
690 Contribution of oxazolidinones to the efficacy of novel regimens containing
691 bedaquiline and pretomanid in a mouse model of tuberculosis. Antimicrob Agents
692 Chemother. 2016;60(1):270–7.

693 5. Conradie F, Diacon AH, Ngubane N, Howell P, Everitt D, Crook AM, et al.
694 Treatment of Highly Drug-Resistant Pulmonary Tuberculosis. N Engl J Med.
695 2020;382(10):893–902.

696 6. Conradie F, Bagdasaryan TR, Borisov S, Howell P, Mikiashvili L, Ngubane N, et
697 al. Bedaquiline–Pretomanid–Linezolid Regimens for Drug-Resistant Tuberculosis.

698 N Engl J Med. 2022;387(9):810–23.

699 7. TB-Alliance. Update on Pretomanid , in Combination with Bedaquiline and
700 Linezolid (the BPaL Regimen) in Drug-Resistant TB. 2022.

701 8. Jackson A. Drugs and the Future: Brain Science, Addiction and Society.
702 Academic Press. 2007.

703 9. Richter E, Rüsch-Gerdes S, Hillemann D. First linezolid-resistant clinical isolates
704 of Mycobacterium tuberculosis. Antimicrob Agents Chemother. 2007;51(4):1534–
705 6.

706 10. Li SY, Converse PJ, Betoudji F, Lee J, Mdluli K, Upton A, et al. Next-Generation
707 Diarylquinolines Improve Sterilizing Activity of Regimens with Pretomanid and the
708 Novel Oxazolidinone TBI-223 in a Mouse Tuberculosis Model. Antimicrob Agents
709 Chemother. 2023;67(4):1–9.

710 11. Holloway WJ. Spectinomycin. Med Clin North Am. 1982;66(1).

711 12. Kanchugl S, Selmer M. Structural Recognition of Spectinomycin by Resistance
712 Enzyme ANT(9) from Enterococcus faecalis. Antimicrob Agents Chemother.
713 2020;64(6):e00371-20.

714 13. Owusu E, Amartey BT, Afutu E, Boafo N. Aminoglycoside Therapy for
715 Tuberculosis: Evidence for Ototoxicity among Tuberculosis Patients in Ghana.
716 Diseases. 2022;10(1):10.

717 14. De Jager R, Van Altena R. Hearing loss and nephrotoxicity in long-term

718 aminoglycoside treatment in patients with tuberculosis. Int J Tuberc Lung Dis.
719 2002;6(7):622–7.

720 15. Temrikar ZH, Kodidela S, Kumar S, Liu J, Robertson GT, Lee RE, et al.
721 Characterization of spectinamide 1599 efficacy against different mycobacterial
722 phenotypes. Tuberculosis [Internet]. 2023;140:1–9. Available from:
723 https://doi.org/10.1016/j.tube.2023.102342

724 16. Lee RE, Hurdle JG, Liu J, Bruhn DF, Matt T, Scherman MS, et al. Spectinamides:
725 A New Class of Semisynthetic Anti-Tuberculosis Agents that Overcome Native
726 Drug Efflux. Nat Med. 2017;20(2):152–8.

727 17. De Vriese AS, Van Coster R, Smet J, Seneca S, Lovering A, Van Haute LL, et al.
728 Linezolid-induced inhibition of mitochondrial protein synthesis. Clin Infect Dis.
729 2006;42(8):1111–7.

730 18. Modongo C, Pasipanodya JG, Zetola NM, Williams SM, Sirugo G, Gumboc T.
731 Amikacin concentrations predictive of ototoxicity in multidrug-resistant
732 tuberculosis patients. Antimicrob Agents Chemother. 2015;59(10):6337–43.

733 19. Liu J, Bruhn DF, Lee RB, Zheng Z, Janusic T, Scherbakov D, et al. Structure-
734 activity relationships of spectinamide antituberculosis agents: A dissection of
735 ribosomal inhibition and native efflux avoidance contributions. ACS Infect Dis.
736 2017;3(1):72–88.

737 20. Bruhn DF, Scherman MS, Liu J, Scherbakov D, Meibohm B, Böttger EC, et al. In
738 vitro and in vivo evaluation of synergism between anti-tubercular spectinamides

739 and non-classical tuberculosis antibiotics. Sci Rep. 2015;5:1–10.

740 21. Robertson GT, Scherman MS, Bruhn DF, Liu J, Hastings C, McNeil MR, et al.
741 Spectinamides are effective partner agents for the treatment of tuberculosis in
742 multiple mouse infection models. J Antimicrob Chemother. 2017;72(3):770–7.

743 22. Gonzalez-Juarrero M, Lukka PB, Wagh S, Walz A, Arab J, Pearce C, et al.
744 Preclinical Evaluation of Inhalational Spectinamide-1599 Therapy against
745 Tuberculosis. ACS Infect Dis. 2021;7(10):2850–63.

746 23. Wagh S, Rathi C, Lukka PB, Parmar K, Temrikar Z, Liu J, et al. Model-based
747 exposure-response assessment for spectinamide 1810 in a mouse model of
748 tuberculosis. Antimicrob Agents Chemother. 2021;65(11):1–15.

749 24. Nirmal A, Sznajder K, Patil R, Shaikh B. Preference of inhalants over
750 pills/injections among pulmonary tuberculosis patients in Western India: A cross-
751 sectional study. J Clin Tuberc Other Mycobact Dis. 2021;23.

752 25. Matthieu B, Matthieu J, Nicolas G, Patrice G, Srine M, William C, et al.
753 Comparison of intrapulmonary and systemic pharmacokinetics of colistin
754 methanesulfonate (CMS) and colistin after aerosol delivery and intravenous
755 administration of CMS in critically ill patients. Antimicrob Agents Chemother.
756 2014;58(12):7331–9.

757 26. Rathi C, Lukka PB, Wagh S, Lee RE, Lenaerts AJ, Braunstein M, et al.
758 Comparative pharmacokinetics of spectinamide 1599 after subcutaneous and
759 intrapulmonary aerosol administration in mice. Tuberculosis. 2019;114:119–22.

760 27. Hickey AJ, Misra A, Fourie PB. Dry powder antibiotic aerosol product
761 development: Inhaled therapy for tuberculosis. J Pharm Sci [Internet].
762 2013;102(11):3900–7. Available from: http://dx.doi.org/10.1002/jps.23705

763 28. Singh AK, Gupta UD. Animal models of tuberculosis: Lesson learnt. Indian J Med
764 Res [Internet]. 2018;147:456–63. Available from:
765 http://www.ncbi.nlm.nih.gov/pubmed/23144490

766 29. De Groote MA, Gilliland JC, Wells CL, Brooks EJ, Woolhiser LK, Gruppo V, et al.
767 Comparative studies evaluating mouse models used for efficacy testing of
768 experimental drugs against Mycobacterium tuberculosis. Antimicrob Agents
769 Chemother. 2011;55(3):1237–47.

770 30. Robertson GT, Ramey ME, Massoudi LM, Carter CL, Zimmerman M, Kaya F, et
771 al. Comparative Analysis of Pharmacodynamics in the C3HeB/FeJ Mouse
772 Tuberculosis Model for DprE1 Inhibitors TBA-7371, PBTZ169, and OPC-167832.
773 Antimicrob Agents Chemother. 2021;65(11):e00583-21.

774 31. Irwin SM, Driver E, Lyon E, Schrupp C, Ryan G, Gonzalez-Juarrero M, et al.
775 Presence of multiple lesion types with vastly different microenvironments in
776 C3HeB/FeJ mice following aerosol infection with Mycobacterium tuberculosis. Dis
777 Model Mech. 2015;8(6):591–602.

778 32. Driver ER, Ryan GJ, Hoff DR, Irwin SM, Basaraba RJ, Kramnik I, et al. Evaluation
779 of a mouse model of necrotic granuloma formation using C3HeB/FeJ mice for
780 testing of drugs against Mycobacterium tuberculosis. Antimicrob Agents

781 Chemother. 2012;56(6):3181–95.

782 33. Lanoix JP, Lenaerts AJ, Nuermberger EL. Heterogeneous disease progression
783 and treatment response in a C3HeB/FeJ mouse model of tuberculosis. Dis Model
784 Mech. 2015;8(6):603–10.

785 34. Harper J, Skerry C, Davis SL, Tasneen R, Weir M, Kramnik I, et al. Mouse model
786 of necrotic tuberculosis granulomas develops hypoxic lesions. J Infect Dis.
787 2012;205(4):595–602.

788 35. Irwin SM, Gruppo V, Brooks E, Gilliland J, Scherman M, Reichlen MJ, et al.
789 Limited activity of clofazimine as a single drug in a mouse model of tuberculosis
790 exhibiting caseous necrotic granulomas. Antimicrob Agents Chemother.
791 2014;58(7):4026–34.

792 36. Aly S, Wagner K, Keller C, Malm S, Malzan A, Brandau S, et al. Oxygen status of
793 lung granulomas in Mycobacterium tuberculosis-infected mice. J Pathol.
794 2006;210:298–305.

795 37. Walter ND, Ernest JP, Dide-Agossou C, Bauman AA, Ramey ME, Rossmassler K,
796 et al. Lung microenvironments harbor Mycobacterium tuberculosis phenotypes
797 with distinct treatment responses . Antimicrob Agents Chemother. 2023;67(9):1–
798 15.

799 38. Tang S, Yao L, Hao X, Zhang X, Liu G, Liu X, et al. Efficacy, safety and tolerability
800 of linezolid for the treatment of XDR-TB: A study in China. Eur Respir J [Internet].
801 2015;45(1):161–70. Available from: http://dx.doi.org/10.1183/09031936.00035114

802 39. Gerson SL, Kaplan SL, Bruss JB, Le V, Arellano FM, Hafkin B, et al. Hematologic
803 effects of linezolid: Summary of clinical experience. Antimicrob Agents
804 Chemother. 2002;46(8):2723–6.

805 40. Mase A, Lowenthal P, True L, Henry L, Barry P, Flood J. Low-Dose Linezolid for
806 Treatment of Patients With Multidrug-Resistant Tuberculosis. Open Forum Infect
807 Dis. 2022;9(12):1–10.

808 41. Bigelow KM, Tasneen R, Chang YS, Dooley KE, Nuermberger EL. Preserved
809 efficacy and reduced toxicity with intermittent linezolid dosing in combination with
810 bedaquiline and pretomanid in a murine tuberculosis model. Antimicrob Agents
811 Chemother. 2020;64(10).

812 42. Bigelow KM, Deitchman AN, Li SY, Barnes-Boyle K, Tyagi S, Soni H, et al.
813 Pharmacodynamic Correlates of Linezolid Activity and Toxicity in Murine Models
814 of Tuberculosis. J Infect Dis. 2021;223(11):1855–64.

815 43. Van Crevel R, Karyadi E, Netea MG, Verhoef H, Nelwan RHH, West CE, et al.
816 Decreased plasma leptin concentrations in tuberculosis patients are associated
817 with wasting and inflammation. J Clin Endocrinol Metab. 2002;87(2):758–63.

818 44. Nikonenko BV, Samala R, Einck L, Nacy CA. Rapid, simple in vivo screen for new
819 drugs active against Mycobacterium tuberculosis. Antimicrob Agents Chemother.
820 2004;48(12):4550–5.

821 45. Pstragowski, M. Zbrzezna, M. and Bujalska-Zadrozny M. Advances in
822 pharmacotherapy of Tuberculosis. Acta Pol - Drug Res [Internet]. 2017;74(1):3–

823 11. Available from:
824 https://www.embase.com/search/results?subaction=viewrecord&id=L604925228&
825 from=export

826 46. Nuermberger EL, Martínez-Martínez MS, Sanz O, Urones B, Esquivias J, Soni H,
827 et al. GSK2556286 Is a Novel Antitubercular Drug Candidate Effective In Vivo
828 with the Potential To Shorten Tuberculosis Treatment. Antimicrob Agents
829 Chemother. 2022;66(6).

830 47. Wasserman S, Denti P, Brust JCM, Abdelwahab M, Hlungulu S, Wiesner L, et al.
831 Linezolid pharmacokinetics in South African patients with drug-resistant
832 tuberculosis and a high prevalence of HIV coinfection. Antimicrob Agents
833 Chemother. 2019;63(3).

834 48. Abebe G, Bonsa Z, Kebede W. Early Safety and Efficacy of Linezolid-Based
835 Combination Therapy among Patients with Drug-Resistant Tuberculosis in
836 North-western Nigeria. Int J Mycobacteriology. 2021;10:129–35.

837 49. Palomino JC, Martin A. Drug resistance mechanisms in Mycobacterium
838 tuberculosis. Antibiotics. 2014;3(3):317–40.

839 50. Sotgiu G, Centis R, D'Ambrosio L, Alffenaar JWC, Anger HA, Caminero JA, et al.
840 Efficacy, safety and tolerability of linezolid containing regimens in treating MDR-
841 TB and XDR-TB: Systematic review and meta-analysis. Eur Respir J.
842 2012;40(6):1430–42.

843 51. Mirlohi M-S, Nezamodini ZS, Rezvani Z, Kian K. Hematological and liver toxicity

844 of anti-tuberculosis drugs. Electron Physician. 2016;8(9):3592–7.

845 52. Kassa E, Enawgaw B, Gelaw A, Gelaw B. Effect of anti-tuberculosis drugs on
846 hematological profiles of tuberculosis patients attending at University of Gondar
847 Hospital, Northwest Ethiopia. BMC Hematol. 2016;16(1):1–11.

848 53. Luo M, Liu M, Wu X, Wu Y, Yang H, Qin L, et al. Impact of anemia on prognosis
849 in tuberculosis patients. Ann Transl Med. 2022;10(6):329–329.

850 54. Iyer SS, Iyer SS, He Q, He Q, Janczy JR, Janczy JR, et al. Mitochondrial
851 Cardiolipin Is Required for Nlrp3 Inflammasome Activation. Immunity [Internet].
852 2013;39(2):311–23. Available from:
853 http://linkinghub.elsevier.com/retrieve/pii/S1074761313003294%5Cnpapers3://pu
854 blication/doi/10.1016/j.immuni.2013.08.001

855 55. Winchell CG, Mishra BB, Phuah JY, Saqib M, Nelson SJ, Maiello P, et al.
856 Evaluation of IL-1 Blockade as an Adjunct to Linezolid Therapy for Tuberculosis in
857 Mice and Macaques. Front Immunol. 2020;11:1–18.

858 56. Elmore SA. Enhanced Histopathology of the Bone Marrow Susan. Toxicol Pathol
859 [Internet]. 2006;34(5):666–86. Available from:
860 https://www.ncbi.nlm.nih.gov/pmc/articles/PMC3624763/pdf/nihms412728.pdf

861 57. Jasenosky LD, Scriba TJ, Hanekom WA, Goldfeld AE. T cells and adaptive
862 immunity to Mycobacterium tuberculosis in humans. Immunol Rev.
863 2015;264(1):74–87.

864 58. Lovewell RR, Baer C, Mishra BB, Smith CM, Christopher M. Granulocytes act as
865 a niche for Mycobacterium tuberculosis growth. Mucosal Immunol.
866 2021;14(1):229–41.

867 59. Stewart IE, Lukka PB, Liu J, Meibohm B, Gonzalez- M, Braunstein MS, et al.
868 Development and Characterization of a Dry Powder Formulation for Anti-
869 Tuberculosis Drug Spectinamide 1599. Pharmacol Res. 2021;36(9):136.

870 60. Lyons MA, Ramey ME, Bauman AA, Pauly S, Rossmassler K, Reid J, et al. Nix-
871 TB regimen in a short-course murine model of tuberculosis. Antimicrob Agents
872 Chemother. 2024;68(5):01010–23.

873 61. Lyons MA. Pharmacodynamics and Bactericidal Activity of Combination
874 Regimens in Pulmonary Tuberculosis: Application to Bedaquiline-Pretomanid-
875 Pyrazinamide. Antimicrob Agents Chemother. 2022;66(12):1–15.

876 62. Dutt TS, Karger BR, Fox A, Youssef N, Dadhwal R, Ali MZ, et al. Mucosal
877 exposure to non-tuberculous mycobacteria elicits B cell-mediated immunity
878 against pulmonary tuberculosis. Cell Rep [Internet]. 2022;41(11):111783.
879 Available from: https://doi.org/10.1016/j.celrep.2022.111783

880 63. Golde WT, Gollobin P, Rodriguez LL. A rapid, simple, and humane method for
881 submandibular bleeding of mice using a lancet. Lab Anim (NY). 2005;34(9):39–
882 43.

883 64. Fox A, Dutt TS, Karger B, Rojas M, Obregón-Henao A, Anderson GB, et al. Cyto-
884 Feature Engineering: A Pipeline for Flow Cytometry Analysis to Uncover Immune

885 Populations and Associations with Disease. Sci Rep. 2020;10(1):1–12.

886

887

888 ## Supporting information

889 **Figure S1 (C3HeB/FeJ Study 1).** Bacterial burden (CFU) in Mtb infected C3HeB/FeJ mice treated with
890 BPaL and BPaS regimen for 4 weeks

891 **Figure S2 (C3HeB/FeJ Study 2).** Bacterial burden (CFU) in Mtb infected C3HeB/FeJ mice treated with
892 BPa, BPaL and BPaS regimen for 4 weeks

893 **Figure S3 (C3HeB/FeJ Study 3).** Bacterial burden (CFU) in Mtb infected C3HeB/FeJ mice treated with
894 BPa, BPaL and BPaS regimen for 4 weeks

895 **Figure S4.** Change in the average body weight of Mtb infected C3HeB/FeJ mice during drug treatment
896 (combined data)

897 **Figure S5 (C3HeB/FeJ Study 1).** Change in the average body weight of Mtb infected C3HeB/FeJ mice
898 during drug treatment

899 **Figure S6 (C3HeB/FeJ Study 2).** Change in the average body weight of Mtb infected C3HeB/FeJ mice
900 during drug treatment

901 **Figure S7 (C3HeB/FeJ Study 3).** Change in the average body weight of Mtb infected C3HeB/FeJ mice
902 during drug treatment

903 **Figure S8 (BALB/c Study 1).** Bacterial burden (CFU) in Mtb infected BALB/c mice treated with BPaL and
904 BPaS regimen for 4 weeks

905 **Figure S9 (BALB/c Study 2).** Bacterial burden (CFU) in Mtb infected BALB/c mice treated with BPaL and
906 BPaS regimen for 4 weeks

907 **Figure S10.** Change in the average body weight of Mtb infected BALB/c mice during drug treatment

908 (combined data)

909 **Figure S11 (BALB/c Study 1).** Change in the average body weight of Mtb infected BALB/c mice during
910 drug treatment

911 **Figure S12 (BALB/c Study 2).** Change in the average body weight of Mtb infected BALB/c mice during
912 drug treatment

913 **Figure S13**. Change in the cytokines and chemokines profile in Mtb infected C3HeB/FeJ mice during drug
914 treatment

915 **Figure S14**. Spearman's correlation analysis between bacterial burden (CFU) and cytokine and
916 chemokine profile in the lungs of Mtb infected C3HeB/FeJ mice treated with BPaL and BPaS regimen
917

918 **Figure S15**. Spearman's correlation analysis between lung bacterial burden (CFU) and plasma cytokine
919 and chemokine profile in Mtb infected C3HeB/FeJ mice treated with BPaL and BPaS regimen
920

921 **Figure S16.** Immune cell populations in the lungs of Mtb infected C3HeB/FeJ TB model after 4 weeks
922 therapy
923

924 **Table S1**. **Reagents**
925

926 **Table S2. Antibodies**